CARS diagnostics of high pressure discharges

J. Uhlenbusch
Institute for Laser and Plasma Physics,
Heinrich-Heine-Universität Düsseldorf

1 Introduction

The availability of laser systems with the choice of pulsed and cw operation, narrow band width, high peak power, and operating in a broad frequency range has made nonlinear scattering processes very attractive for a nonintrusive in situ diagnostic of a plasma. Amongst other nonlinear techniques, Coherent Anti-Stokes Raman Scattering (CARS) and its variants resonance enhanced CARS (RECARS) and polarization CARS (POLCARS) are effective tools to determine the density, kinetic and population temperatures of discharges containing a reasonable quantity for instance of molecular species. Thus CARS experiments today are often performed to examine the non-equilibrium state of a plasma by measuring the CARS intensity from rovibronic transitions for a multitude of quantum levels. Furtherly, they are useful to validate the results of plasma modelling, and finally, they indirectly allow to determine the electron density by measuring the population density of vibrational states, if they are mainly populated by electron collisions.

CARS is a very universal diagnostic technique useful to understand molecular properties, but its use requires large-scale expenditures. One needs at least two high quality laser systems making high demands on stability, power level, mode behaviour, bandwidth and coherence. An extensive numerical program for calculations of molecular energy levels, folding and fit procedures has to accompany the experiments.

After a short description of the principles of the CARS, RECARS and POLCARS techniques and a discussion of setups for CARS experiments some experimental results are summarized. The results concern mainly plasma under atmospheric pressure, in particular the determination of temperature in a CO_2 laser-induced pyrolysis flame burning in a silane-acetylene gas mixture, the measurements of N_2 vibrational and rotational temperatures as well as the electron density by CARS and of an NO minority by POLCARS in an atmospheric microwave discharge, and finally RECARS experiments on indium iodide, which is present in metal halide discharge lamps. Guided by these examples some problems and difficulties arising when performing CARS measurements are discussed.

2 Basics of CARS processes

2.1 Principle

CARS is a coherent four-wave mixing process, where three laser beams, two pump beams (ω_P and ω'_P) and the Stokes beam (ω_S) overlap in the medium under investigation. By nonlinear interaction with the molecules a fourth coherent beam with the anti-Stokes frequency $\omega_{AS} = \omega_P - \omega_S + \omega'_P$ is generated, whenever the difference frequency $\omega_P - \omega_S$ coincides with a molecular Raman transition frequency $\omega_{\beta\alpha}$. If additionally one of the pump frequencies is tuned to a suitable electronic resonance frequency one obtains an electronic resonance enhancement of the CARS signal and hence a higher sensitivity than in ordinary CARS; this technique is named RECARS. In case of (frequency) degenerate CARS the two pump beams are produced by the same laser, i. e. $\omega_P = \omega'_P$.

The CARS process can be visualized in a molecular energy level diagram as depicted in fig. 1. Here $|\,\alpha\,\rangle$ and $|\,\beta\,\rangle$ are molecular rovibrational states, while $|\,\gamma\,\rangle$ and $|\,\delta\,\rangle$ are virtual levels. The two-photon transition $|\,\alpha\,\rangle \longrightarrow |\,\beta\,\rangle$ stimulated by the Stokes beam has to fulfill the selection rules of the ordinary

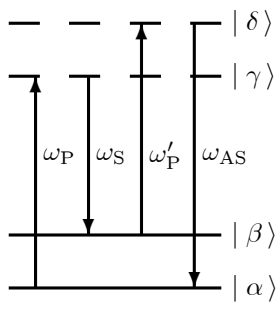

Figure 1: Energy level diagram of the CARS process.

Raman effect, which are in case of a diatomic molecule:

$$\Delta v = 1, \Delta J = \begin{cases} -2 & : \text{ O branch} \\ 0 & : \text{ Q branch} \\ +2 & : \text{ S branch}\,. \end{cases} \tag{1}$$

CARS as a coherent scattering process has to fulfill a phase matching condition, which is equivalent to momentum conservation of the photons involved. With the wave vectors of the two pump beams ($\underline{k}_{\mathrm{P}}$ and $\underline{k}'_{\mathrm{P}}$) and the Stokes beam ($\underline{k}_{\mathrm{S}}$) the wave vector of the Raman signal can be written

$$\underline{k}_{\mathrm{AS}} \;=\; \underline{k}'_{\mathrm{P}} + (\underline{k}_{\mathrm{P}} - \underline{k}_{\mathrm{S}}) \iff \underline{k}_{\mathrm{P}} + \underline{k}'_{\mathrm{P}} \;=\; \underline{k}_{\mathrm{S}} + \underline{k}_{\mathrm{AS}}\,. \tag{2}$$

In order to satisfy relation (2) two different arrangements are customarily used. In low dispersive media collinear beams are sufficient for phase matching (see fig. 2a). Better spatial resolution is obtained with the 'folded BoxCARS' arrangement, a 3-dimensional phase matching geometry. The respective $\underline{k}$-vector diagram is depicted in fig. 2b); fig. 2c) shows its experimental realization. Finally, fig. 2d) displays a scheme called degenerate four-wave mixing (DFWM), which requires only a single tunable laser as light source. This technique is not discused in the following.

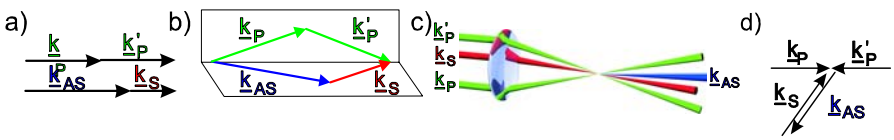

Figure 2. Phase matching in CARS: a) collinear CARS; b) folded BoxCARS; c) experimental realization of b), d) degenerate four-wave mixing with $|\underline{k}_{\mathrm{P}}| = |\underline{k}'_{\mathrm{P}}| = |\underline{k}_{\mathrm{S}}| = |\underline{k}_{\mathrm{AS}}|$.

There are two different methods of measuring a CARS spectrum. In scanning CARS a narrow bandwidth Stokes laser (spectral width typical < 0.1 cm^{-1}) is tuned over the Raman resonances of the probed species. The spectral resolution of this technique is mainly determined by the bandwidth of the applied lasers. Scanning CARS is a suitable diagnostic for steady or at least reproducible plasmas. In broadband or multiplex CARS a broadband dye laser (spectral width typical 100 cm^{-1}) is used to pump all Raman transitions under investigation simultaneously. The spectral resolution of this method is achieved by using a monochromator and a multichannel detection system. Thus, one laser shot is sufficient to measure a whole CARS spectrum. Spectral resolution and sensitivity of this technique, however, are poorer than in scanning CARS.

For a detailed study the articles [1, 2, 3] are recommended.

2.2 Theory of CARS process

The strong laser fields cause a nonlinear polarization of the medium under investigation:

$$\underline{P}(\underline{r},t) = \epsilon_0\chi^{(1)} \cdot \underline{E}(\underline{r},t) + \epsilon_0\chi^{(2)} : \underline{E}(\underline{r},t)\underline{E}(\underline{r},t) + \epsilon_0\chi^{(3)} : \underline{E}(\underline{r},t)\underline{E}(\underline{r},t)\underline{E}(\underline{r},t) + \ldots\,, \tag{3}$$

The third order part of the polarization has a frequency component oscillating with the anti-Stokes frequency ω_{AS}:

$$\underline{P}^{(3)}(\omega_{\mathrm{AS}}) \;=\; \epsilon_0\underline{\chi}^{(3)}(\omega_{\mathrm{AS}};\omega_{\mathrm{P}},-\omega_{\mathrm{S}},\omega'_{\mathrm{P}})\,\underline{E}_{\mathrm{P}}\underline{E}^*_{\mathrm{S}}\underline{E}'_{\mathrm{P}}\exp[-i(\omega_{\mathrm{P}}-\omega_{\mathrm{S}}+\omega'_{\mathrm{P}})t], \tag{4}$$

which is the source of the CARS signal.

The respective third order nonlinear susceptibility $\chi^{(3)}$ is a tensor of fourth rank with 81 complex components. For isotropic media like liquids, gases and plasmas symmetry considerations reduce the number of components to three independent contributions.

If all applied electric fields have the same direction of polarization only one complex function determines $\chi^{(3)}$. Additionally, $\chi^{(3)}$ may split up into a contribution with resonant terms and a nonresonant part,

$$\chi^{(3)} = \chi_R^{(3)} + \chi_{NR}^{(3)} \,. \tag{5}$$

The resonant contribution $\chi_R^{(3)}$ can be written [4]

$$\chi_R^{(3)}(\omega_{\mathrm{AS}};\omega_{\mathrm{P}},-\omega_{\mathrm{S}},\omega'_{\mathrm{P}}) = \frac{n\epsilon_0}{4\pi^2\hbar}\left(\frac{2\pi c}{\omega_{\mathrm{S}}}\right)^4 \sum_{\alpha,\beta}\left(\frac{\mathrm{d}\sigma_{\beta\alpha}}{\mathrm{d}\Omega}\right)_{ij}\left(\varrho_{\alpha\alpha}^{(0)} - \varrho_{\beta\beta}^{(0)}\right)$$

$$\times \int_{-\infty}^{\infty} f(v_z)\left[\frac{1}{\omega_{\beta\alpha} - (\omega_{\mathrm{P}} - \omega_{\mathrm{S}}) + (k_{\mathrm{P}} - k_{\mathrm{S}})v_z - i\Gamma_{\beta\alpha}} + \frac{1}{\omega_{\beta\alpha} - (\omega'_{\mathrm{P}} - \omega_{\mathrm{S}}) + (k'_{\mathrm{P}} - k_{\mathrm{S}})v_z - i\Gamma_{\beta\alpha}}\right] dv_z$$

$$= i\frac{n\epsilon_0}{4\pi^{3/2}\hbar}\left(\frac{2\pi c}{\omega_{\mathrm{S}}}\right)^4 \sum_{\alpha,\beta}\left(\frac{\mathrm{d}\sigma_{\beta\alpha}}{\mathrm{d}\Omega}\right)\left(\varrho_{\alpha\alpha}^{(0)} - \varrho_{\beta\beta}^{(0)}\right)$$

$$\times \frac{1}{\Delta\omega_{\mathrm{D}}^{\beta\alpha}}\left[w\left(\frac{1}{\Delta\omega_{\mathrm{D}}^{\beta\alpha}}(\omega_{\mathrm{P}} - \omega_{\mathrm{S}} - \omega_{\beta\alpha} + i\Gamma_{\beta\alpha})\right) + w\left(\frac{1}{\Delta\omega_{\mathrm{D}}^{\beta\alpha}}(\omega'_{\mathrm{P}} - \omega_{\mathrm{S}} - \omega_{\beta\alpha} + i\Gamma_{\beta\alpha})\right)\right], \tag{6}$$

where w is the complex error function,

$$\Delta\omega_{\mathrm{D}}^{\beta\alpha} = \omega_{\beta\alpha}\left(\frac{2k_{\mathrm{B}}T_{\mathrm{gas}}}{mc^2}\right)^{1/2} \tag{7}$$

is the Doppler width (half width of 1/e mean) of the Raman transition $|\,\alpha\,\rangle \longrightarrow |\,\beta\,\rangle$, $(\mathrm{d}\sigma_{\beta\alpha}/\mathrm{d}\Omega)$ designates the Raman cross section, $\omega_{\beta\alpha}$ and $\Gamma_{\beta\alpha}$ are the respective frequency and collisional line width (half width of half mean). n stands for the density of the probed species, ϱ_α and ϱ_β describe the relative population densities of the molecular levels involved in the Raman transition. This formula is restricted to the case that saturation (see below) is absent and Doppler and pressure broadening are the dominant broadening processes. The resonant part $\chi_R^{(3)}$ includes the lines specific for the medium under investigation and gives the information needed for the evaluation of temperatures and densities by means of the diagnostic technique CARS.

The nonresonant part $\chi_{NR}^{(3)}$ originates from far away resonances and shows only a poor frequency dependence. It is found for atomic species, like noble gases, too, and nonresonant scattering from a well known number of scatterers is often used for calibration purposes.

To calculate a CARS spectrum the square of the modulus of $\chi^{(3)}$ has to be convoluted with the spectral laser profiles:

$$I_{\mathrm{AS}} \sim \int\int\int |\chi^{(3)}(\omega_{\mathrm{AS}};\omega_{\mathrm{P}},-\omega_{\mathrm{S}},\omega'_{\mathrm{P}})|^2 I_{\mathrm{P}}(\omega_{\mathrm{P}}) I_{\mathrm{S}}(\omega_{\mathrm{S}}) I'_{\mathrm{P}}(\omega_{\mathrm{P}\prime})\,\mathrm{d}\omega_{\mathrm{P}}\mathrm{d}\omega_{\mathrm{S}}\mathrm{d}\omega'_{\mathrm{P}}\,. \tag{8}$$

Applying the selection rules (1) one obtains from the energy eigenvalues of rovibrational levels of a diatomic molecule the frequencies of the Q branch Raman resonances:

$$\omega_{v,J} = \omega_e - 2(v+1)\omega_e x_e - \alpha_e J(J+1) + \ldots\,. \tag{9}$$

The branch belonging to the fundamental vibrational transition $|\,v=0\,\rangle \longrightarrow |\,v=1\,\rangle$ is named 'cold band', the higher vibrational transitions $|\,v>0\,\rangle \longrightarrow |\,v+1\,\rangle$ are called 'hot bands'.

The population density $\overset{(0)}{\varrho}_{v,J}$ of a rovibrational level $|\,v,J\,\rangle$ is given in case of LTE by the Boltzmann factor

$$\overset{(0)}{\varrho}_{v,J} = \frac{g_I(2J+1)}{Z}\exp\left(-\frac{E_{v,J}}{k_{\mathrm{B}}T}\right) \tag{10}$$

where T might be different for vibrational and rotational states. Here Z denotes the partition function, g_I is the nuclear spin statistic weight.

The population densities of upper and lower states can be redistributed by the competitive processes of stimulated Raman scattering (SRS) and optical Stark effect. The SRS process splits a resonance line belonging to a molecular Raman transition into two broadened satellites. The dynamical Stark effect splits the levels with respect to the magnetic quantum number m and causes line shift and line broadening. Relaxing collisions repair partly the distortion of population densities by SRS processes and Stark effect.

2.3 Polarization CARS (POLCARS)

In most experiments all CARS beams and signals are assumed to be polarized in the same direction. If the directions of polarization are changed, the resonant and nonresonant parts of the CARS signal show different dependencies on polarization, and nonresonant contributions can be suppressed. This is utilized by the polarization CARS technique (POLCARS) [3, 5, 6] to reduce the non–resonant CARS background generated by majority species. Only a short overview concerning POLCARS is given here. The third order polarization can be written as

$$\underline{P}^{(3)}(\omega_{\mathrm{AS}}) \sim \left[\chi_1^{(3)}(\underline{E}_S^* \cdot \underline{E}_{P_2})\underline{E}_{P_1} + \chi_2^{(3)}(\underline{E}_{P_1} \cdot \underline{E}_{P_2})\underline{E}_S^* + \chi_3^{(3)}(\underline{E}_{P_1} \cdot \underline{E}_S^*)\underline{E}_{P_2}\right], \tag{11}$$

where in case of equal pump frequencies $\omega_{\mathrm{P}_1} = \omega_{\mathrm{P}_2}$ (degenerate CARS) the susceptibilities obey the relation $\chi_1^{(3)} = \chi_3^{(3)}$. Introducing a Cartesian coordinate system, which is properly oriented against the directions of polarization and of the wave vectors of incident laser beams one has

$$\chi_1^{(3)} = \chi_{xxyy}^{(3)}, \chi_2^{(3)} = \chi_{xyxy}^{(3)}, \chi_3^{(3)} = \chi_{xyyx}^{(3)}. \tag{12}$$

Splitting up the susceptibilities into a resonant and a non–resonant part, equat. (5) has to be rewritten as $\chi_i^{(3)} = \chi_{i,\mathrm{R}}^{(3)} + \chi_{i,\mathrm{NR}}^{(3)}$ $(i = 1, 2, 3)$. The non–resonant part generally fulfills the so called Kleinman's symmetry as the resonant one does far away from the line center.

$$\chi_{\mathrm{NR},1}^{(3)} = \chi_{\mathrm{NR},2}^{(3)} = \chi_{\mathrm{NR},3}^{(3)}. \tag{13}$$

This relation therefore is well validated, if the spectral distance to the neighboured resonances is large compared to their line width.

In case of resonance the inequality

$$\chi_{\mathrm{R},1}^{(3)}, \chi_{\mathrm{R},3}^{(3)} \gg \chi_{\mathrm{R},2}^{(3)} \tag{14}$$

is valid for nearly entirely polarized lines, in particular for light molecules. The case $\chi_{\mathrm{R},2}^{(3)} = 0$ means complete linear polarization of the resonance line under investigation. Differences in the susceptibilities $\chi_{\mathrm{R}}^{(3)}$ and $\chi_{\mathrm{NR}}^{(3)}$ lead via equat. (11) to a different polarization state of the non–resonant and resonant contributions. If the incoming beams are not polarized in the same direction, the non–resonant contribution can be eliminated by using an analyzer in front of the detector. Furtherly, by a proper choice of the direction of polarization the non-resonant contribution can be even completely suppressed [6].

2.4 RECARS

In case of electronic resonant CARS (RECARS) at least three of the four energy levels shown in fig. 1 are in resonance. A proper tuning of pump and Stokes laser to these resonances requires (instead of using one frequency-fixed pump laser and one tunable Stokes laser in case of CARS) now two frequency-tunable lasers. By proper choice of the pump and Stokes frequency the rovibrational Raman spectrum of the molecular species under investigation is detectable in the visible or near UV-regime. The CARS theory given in section 2.2 for the calculation of $\overset{(3)}{\chi}$ must be considerably modified, because much more resonance denominators contribute as are considered when evaluating equat. (6). With the new denotation $\omega_4 = \omega_{as}, \omega_1 = \omega_p, \omega_2 = \omega_s, \omega_3 = \omega_p'$ the susceptibility may now be written

$$\chi_{ijkl}^{(3)}(\omega_4; \omega_1, -\omega_2, \omega_3) = \frac{n}{4\hbar^3\epsilon_0} \sum_{\alpha,\beta,\gamma,\delta} \int_{-\infty}^{\infty} f(v_z)\,[A - B + C - D]\,dv_z \tag{15}$$
$$+ \{(j, \omega_1, k_1) \leftrightarrow (l, \omega_3, k_3)\}.$$

Species	$^{14}N_2$	$^{1}H_2$	$^{2}D_2$	$^{16}O_2(\chi^3\sum_g^-)$	$^{16}O_2(a^1\Delta_g)$	$^{12}C^{16}O$	$^{12}C^{16}O_2(\nu_1)$	$^{12}CH_4(\nu_1)$
Stokes λ_s/nm	607.3	683.0	632.5	580.0	577.6	600.5	571.0	629.7
anti-Stokes λ_{as}/nm	473.3	435.7	459.1	491.4	493.1	477.6	498.0	460.5

Table 1: All entries are valid for a pump wavelength $\lambda_p = 532$ nm.

where

$$
\begin{aligned}
A &= \rho^{(0)}_{\alpha\alpha}\mu_{\alpha\delta,i}\mu_{\delta\beta,l}\mu_{\beta\gamma,k}\mu_{\gamma\alpha,j}\,[[\omega_{\gamma\alpha}-\omega_1+k_1v_z-i\Gamma_{\gamma\alpha}] \\
&\quad\times[\omega_{\beta\alpha}-(\omega_1-\omega_2)+(k_1-k_2)v_z-i\Gamma_{\beta\alpha}]\,[\omega_{\delta\alpha}-\omega_4+k_4v_z-i\Gamma_{\delta\alpha}]]^{-1}\ , \\
B &= \rho^{(0)}_{\beta\beta}\mu_{\alpha\delta,i}\mu_{\delta\beta,l}\mu_{\beta\gamma,k}\mu_{\gamma\alpha,j}\,[[\omega_{\gamma\beta}-\omega_2+k_2v_z+i\Gamma_{\gamma\beta}] \\
&\quad\times[\omega_{\beta\alpha}-(\omega_1-\omega_2)+(k_1-k_2)v_z-i\Gamma_{\beta\alpha}]\,[\omega_{\delta\alpha}-\omega_4+k_4v_z-i\Gamma_{\delta\alpha}]]^{-1}\ , \\
C &= \rho^{(0)}_{\beta\beta}\mu_{\alpha\delta,i}\mu_{\delta\beta,j}\mu_{\beta\gamma,k}\mu_{\gamma\alpha,l}\,[[\omega_{\delta\beta}-\omega_3+k_3v_z-i\Gamma_{\delta\beta}] \\
&\quad\times[\omega_{\delta\gamma}-(\omega_3-\omega_2)+(k_3-k_2)v_z-i\Gamma_{\delta\gamma}]\,[\omega_{\delta\alpha}-\omega_4+k_4v_z-i\Gamma_{\delta\alpha}]]^{-1}\ , \\
D &= \rho^{(0)}_{\beta\beta}\mu_{\alpha\delta,i}\mu_{\delta\beta,j}\mu_{\beta\gamma,k}\mu_{\gamma\alpha,l}\,[[\omega_{\gamma\beta}-\omega_2+k_2v_z+i\Gamma_{\gamma\beta}] \\
&\quad\times[\omega_{\delta\gamma}-(\omega_3-\omega_2)+(k_3-k_2)v_z-i\Gamma_{\delta\gamma}]\,[\omega_{\delta\alpha}-\omega_4+k_4v_z-i\Gamma_{\delta\alpha}]]^{-1}\ .
\end{aligned}
\tag{16}
$$

and μ means the molecular dipole moment, see [7].

The expression in braces symbolizes additional terms, which are generated by simultaneous exchange of the Cartesian indices j and l, the frequencies ω_1 and ω_3, and the wave vectors k_1 and k_3.

3 Setups for CARS, POLCARS and RECARS experiments

3.1 CARS

An example of a scanning CARS set-up is given in fig. 3. It consists of a frequency doubled seeded Nd:YAG laser delivering a pulse energy of 100 mJ at $\lambda_P = 532$ nm, which provides the two CARS pump beams and pumps a narrow bandwidth dye laser ($\Delta\omega \approx 0.03$ cm^{-1}) delivering the tunable Stokes beam. The wavelength of the dye laser depends on the choice of the molecule under investigation. A list of wavelengths for the Stokes beam required to get a CARS signal and for the anti-Stokes beam is given in table 1.

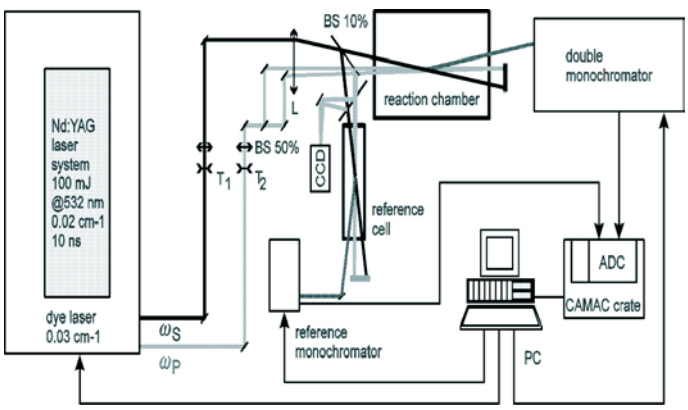

Figure 3. Experimental set-up of a scanning CARS diagnostic system.

The three laser beams are focused into the plasma (reaction chamber) by the lens L ($f = 1$ m) under appropriate BoxCARS angles ($\alpha = 1.43°$) (see fig. 2b) to fulfill the phase matching condition (equat.

(2)). The CARS signal beam generated there is detected by means of a double monochromator serving as a tunable narrow bandwidth filter and a photomultiplier behind it.

A beam splitter (BS 10 %) produces a secondary CARS focus in a reference cell filled with argon. The nonresonant CARS signal generated here (see section 2.2) is utilized to compensate for all kinds of fluctuations in laser power and overlap of the three beams.

A third CARS focus on a CCD camera is useful to monitor and optimize the overlap of the beams.

The wavelength of the Stokes beam may be absolutely calibrated by means of a galvatron or wavemeter. Thus the frequency position of the selected anti-Stokes lines can be found very easily.

Preparatory work must be done to make the CARS system fit for measurements. In a first step nonresonant CARS signals, e.g. from argon, are generated in the reference cell and in the actual CARS focus as function of the frequency of the Stokes beam over an appropriate frequency range. The ratio of the two signals is constant in case of a good alignment of the scattering system.

A second step determines the size of the volume of CARS signal production by means of a thin flat piece of glass moved through the focal zone. This technique allows to find the spatial resolution of the CARS measurement.

Finally, the pulse energy of the three beams must be chosen in a proper way to avoid saturation effects by the competitive processes of stimulated Raman scattering (SRS) and optical Stark effect, see section 2.2. A careful check of the influence of the laser beam intensities without alteration of the laser beam profiles in the CARS focus is performed by using an attenuator consisting of two glass plates, whose mutual planes of inclination can be changed.

3.2 POLCARS

Using POLCARS two Soleil-Babinet components must be integrated into the incoming beams to adjust the directions of polarization relatively to each other. In order to reject unwanted nonresonant CARS signals an analyzer should be aligned in front of the double monochromator.

3.3 RECARS

To meet the resonances of the indium-iodide molecules properly for RECARS application a frequency-tripled Nd:YAG laser at $\lambda = 355$ nm is utilized as pump source for two tunable dye lasers, which oscillate near $\lambda = 412$ nm. These two dye lasers operating both with the dye Exalite 411 in Dioxan with an optimum energy conversion of 6.5 % corresponding with a beam energy of 4.5 mJ serve as pump and Stokes laser, resp., in a frequency-degenerate RECARS setup ($\omega_p = \omega_p'$). Both dye lasers have been individually designed for scanning CARS measurement, such that high beam-pointing stability, good beam profile, and small spectral width is combined with high power output.

When frequency degenerate RECARS is performed, in general only double resonances are adjustable with the laser system. Therefore according to the choices of the laser frequencies, in the resonance denominators in equat. (15) only two terms can be made to zero at the same time (regardless of the imaginary part). In general, each set of four energy levels leads to five double resonances at frequency degenerate RECARS. In the Raman-pump-frequency plane, they lie at the edges and in the middle point of a square, respectively. Calculating the rovibronic energy values some additional and interesting results are achieved. There are areas where the five points in the plane grow together with varying J and meet in one point. This means that for a certain set of transitions allowed by the selection rules and a certain (high) rotational quantum number J, triple resonant RECARS is possible even with frequency degenerate RECARS, because the frequencies $\omega_{\beta\alpha}$ and $\omega_{\delta\gamma}$ are equal in those cases. In general the heavy molecules have closely spaced rotational and vibrational energy levels. Therefore in the scanning range of the laser system many double resonances occur and in a mixture of different additives typical for halide lamps such as InI, HgI, TlI, etc. selectivity is very limited with double resonant RECARS. The spectral points with triple resonances are like a fingerprint for the respective molecule.

A careful check of saturation effects by the technique described in section 3.1 is imperative.

4 Experimental results

The following sections compile CARS measurements as they are representative of experiments near atmospheric pressure. The examples should illustrate the ability of this technique with respect to its sensitivity

and high spatial and temporal resolution even in a dusty environment.

4.1 Temperature and density measurements in a pyrolysis flame

In flames or plasma experiments often very steep temperature gradients are found, which are responsible for a certain heating rate of species passing such zones. This heating rate is very important to characterize chemical processes, in particular the generation of nanosized particles in a pyrolytic flame. Powders for special bulk ceramic applications should be characterized by a small particle size, extremely narrow sized distribution, weak agglomeration, spherical particle form and high degree of purity. All theses criteria may be satisfied by the method of laser pyrolysis introduced here. Our experiments are closely related to early innovative experiments in [8]. By several improvements, however, we could step up the powder production rates for an order of magnitude.

A scheme of the laser pyrolytic experiment is shown in fig. 4. Main feature is a stainless steel reaction chamber with its central inlet nozzle for the reactant gas flow. An argon flow is used as protective gas to shield the reaction gas flow from the chamber walls and windows. Above the nozzle tip a CO_2 laser beam is focussed by a cylindrical lens to a horizontal line. The vertical stream of reactant gases interacts the focus line and forms a hot, luminescent reaction zone sustained by absorption processes of the gas under study. In our experiment we use gas mixtures of silane (SiH_4) and acetylene (C_2H_2) or C_2H_4 with $< 3\%$ vol% diboran (B_2H_6) admixtures at 0.5 bar. As final products of the chemical reactions the SiC or boron doped SiC clusters and the gaseous H_2 form the particulate plume.

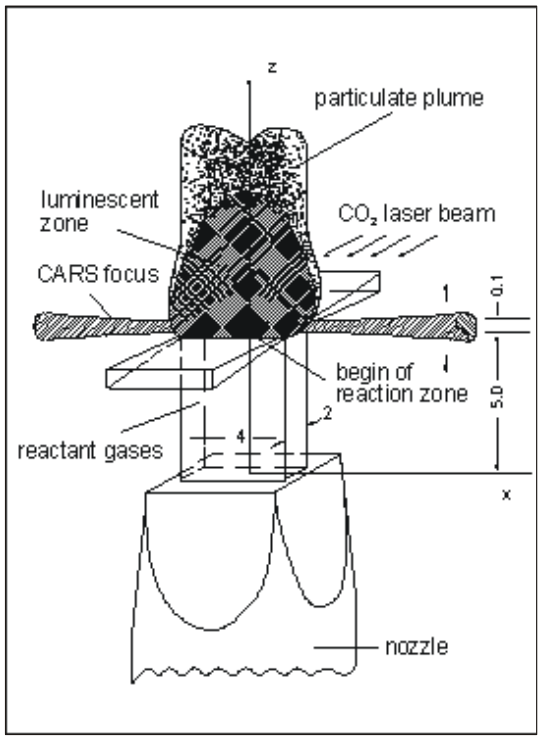

Figure 4. Scheme of the reaction zone (values in mm)

Spatial distribution of rotational temperatures and molecular number densities of C_2H_2 and H_2 were measured with CARS during the production of ultrafine SiC powders. For evaluation of these parameters the experimentally determined CARS spectra are adapted to theoretical spectra of C_2H_2 and H_2 taking account of the nonresonant background in the spectra and the effect of cross-coherence due to the spectral width of the CARS lasers. The study of H_2 Raman line width for the Q(0) and Q(1) vibrational transitions gave no evidence for Dicke narrowing, see [9].

A remarkable feature of the pyrolysis flame is its steep temperature gradient resulting from the small dimensions of the CO_2 laser focal line (0.1 mm) in flow direction, see fig. 4. Due to this gradient, the problem arises that the CARS signal generated in the sample volume does not correspond to a single temperature, but is composed of CARS signals from gas volumes at different temperature. This effect can be minimized by alignment of the sample volume parallel to the CO_2 laser focus line. Following

[10] a model temperature gradient moved through a cylindrical sample volume is treated. The gradient is restricted to the cylinder axis and the CARS intensity distribution within the cylinder of length δ is a Gaussian one. As a criterion for the temperature error induced by spatial averaging they define a parameter G by

$$G = T_0 \left(\frac{\delta}{T_m^2} \frac{dT_m}{dx} \right)_{\delta/2} . \tag{17}$$

T_m being the spatially averaged temperature measured with CARS, T_0 the temperature at the lower-temperature end of the sample volume and x the coordinate parallel to the sample volume cylinder axis. According to this definition, spatial averaging comes close to the true temperature in the sample volume center if $G < 0.1$. In case of a linear temperature gradient, the error in the temperature measurement follows from

$$\frac{\Delta T}{T_m} = 1 - \frac{\left(1 - \frac{G}{2}\right) ln \left(\frac{1}{1-G}\right)}{G}. \tag{18}$$

A numerical evaluation, see [9] gives an $\Delta T/T_m$ of 0.2% in x-direction and 9% in z-direction, see fig. 4.

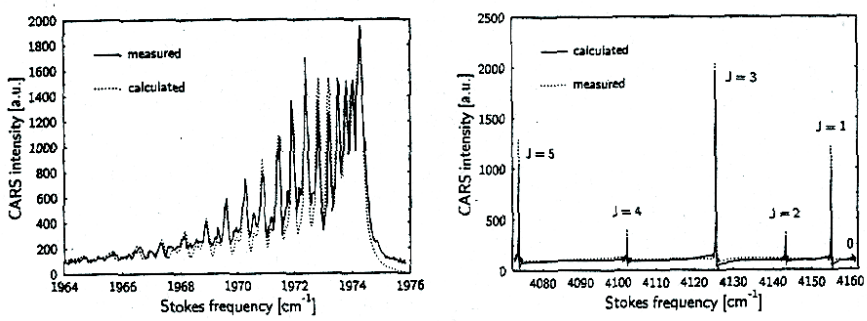

Figure 5. a) CARS spectrum of ν_2 (C_2H_2) recorded in the SiH_4/C_2H_2 reaction flame and comparison with theoretical spectrum b) CARS spectrum of H_2 recorded in the SiH_4/C_2H_4 reaction flame and comparison with theoretical spectrum

A few results may illustrate the efficiency of the CARS measurements in a dusty surrounding. In fig. 5a and 5b experimental and theoretical CARS spectra of ν_2 (C_2H_2) and hydrogen are plotted. The fit of the theoretical spectrum delivers the rotational temperature, which is nearly equal to the gas temperature. The evaluation of the molecular density n was performed according to the fundamental proportionality (which holds for negligible nonresonant background in the spectra, see equats. 6 and 8)

$$I_{as}(n,T) \propto n^2 \left[\sum_J \Delta\varrho_{vJ}(\tau) \right]^2 , \tag{19}$$

where I_{as} is the integral intensity of the experimental CARS spectrum, $\Delta\varrho_{vJ}(T)$ is the difference of the population densities for the Raman transitions ω_{vJ} and the sum contains all transitions which appear in the spectrum. Referencing is performed by taking a spectrum on a cold gas of known temperature T_0 and density n_0. Then

$$n = \sqrt{\frac{I_{as}(n,T)}{I_{as}(n_0,T_0)} \frac{\sum_J \Delta\varrho_{vJ}(T_0)}{\sum_J \Delta\varrho_{vJ}(T)}} n_0. \tag{20}$$

In fig. 6a and 6b temperature and density profiles for C_2H_2 and H_2 versus z-direction are shown, which means across the reaction zone. The data of fig. 6b belong to a higher CO_2 laser power than those in fig. 6a.

As a result of these experiments one concludes that in such laser pyrolysis experiments temperature gradients of 1.6×10^6 K/m are required. The exothermic dissociation of acetylene occurs already at moderate gas temperatures (400^0 C). Further results concern the cluster formation, for more details see [9, 11].

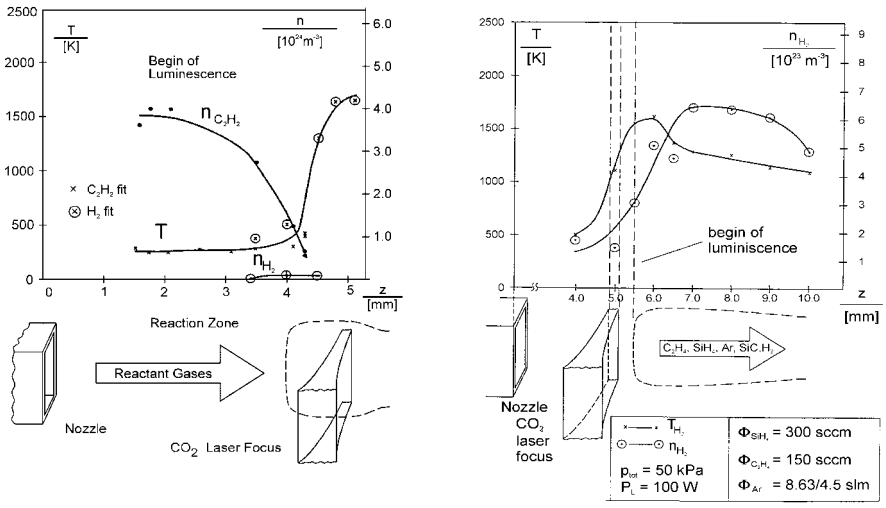

Figure 6. a) Axial temperature and density profiles for C_2H_2 and H_2 in the SiH_4/C_2H_2 reaction flame. Laser power 25 W, $\Phi_{SiH_4} = 120$ sccm, $\Phi_{C_2H_2} = 60$ sscm b) Axial temperature and density profiles for C_2H_2 and H_2 in the SiH_4/C_2H_4 reaction flame. Laser power 100 W, $\Phi_{SiH_4} = 300$ sccm, $\Phi_{C_2H_4} = 150$ sccm

4.2 CARS applied to an atmospheric microwave discharge

Microwave discharges at atmospheric pressure find an increasing number of applications in plasma processing among others because of the lack of electrodes and the comparatively high density of charge carriers and radicals. We have studied in the past cw and pulsed microwave discharges with the aim to reduce NO and NO_2 in exhaust gases. Whilst a cw discharge operated in a pure N_2/NO mixture with a plasma near LTE has a high potential to decompose the NO molecule, the addition of O_2 even at a low percentage leads to a considerable production of NO_x. This is well known from other plasma reduction techniques, but because O_2 is usually present in the exhaust of engines this oxidative path should be avoided [12, 13].

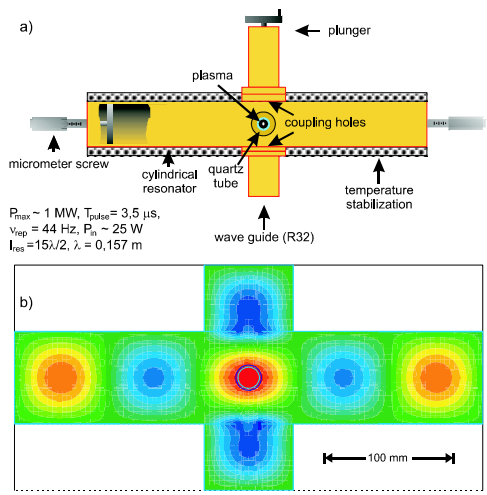

Figure 7. a) Scheme of the 3 GHz microwave discharge b) Field distribution in the 3 GHz resonator calculated with the MAFIA code

Pulsed microwave discharges in non-LTE states allow NO reduction even under 10% O_2 presence. These discharges experience in the starting phase very high values of E/N (reduced field strength) with

a high production rate of neutral N atoms. At the same time the gas temperature remains low and the process $N + O_2 \rightarrow NO + O$ responsible for the NO production is not activated.

A scheme of the pulsed microwave discharge excited by a magnetron operated at 3 GHz with a typical repetition rate of 45 Hz is shown in fig. 7a. The actual discharge is embedded in a cylindrical copper resonator, whose length is thermally stabilized and can be tuned to resonance. A length of 15/2 $\lambda(\sim 1\text{m})$ is sufficient to allow for an energy input of 80 mJ/pulse in pure N_2 and of 0.5 J/pulse in an $N_2/O_2/NO$ mixture at a quality factor $Q \simeq 20000$ and a pulse peak power of say 1 MW. The resonator and the wave guide system are filled with SF_6 to suppress unwanted breakdown. The discharge ignites in a quartz tube, which intersects perpendicularly the cylindrical resonator in the middle. The working gas $N_2/O_2/NO$ is fed into the discharge volume with a flow rate of 6-30 slm in tangential direction through 8 small holes. An optimized gas flow is crucial to achieve a high NO reduction rate.

A unidirectional rectifier in the waveguide and a short linear antenna in the resonator allow to measure the electric field strength, which serves for ignition and sustains the subsequent pulsed discharge. Typical results for a pure N_2 discharge and a $N_2/O_2/NO$ mixture are shown in fig. 8a and 8b.

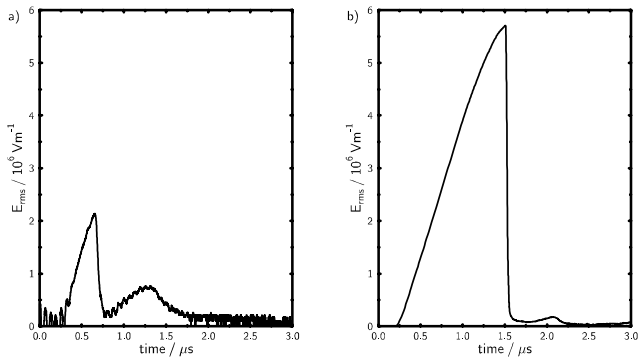

Figure 8. a) Temporal development of the electrical field strength in the discharge tube for pure N_2. Notice the second ignition peak. b) In an $N_2/O_2/NO$ (500 ppm NO, 10% O_2) the maximum electrical field is about a factor of 2-3 higher and no reignition occurs. p=100kPa.

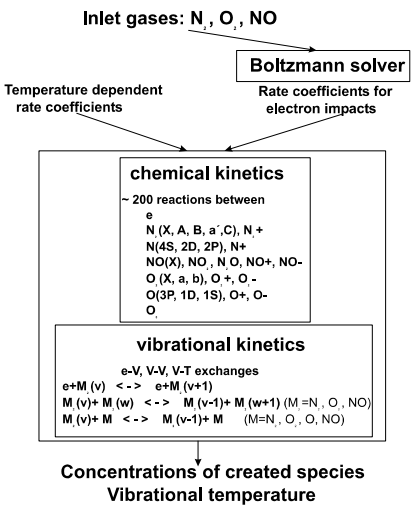

Figure 9. Flow sheet of the plasma model used

The measured time dependent electric field E(t) has a key position for the plasma modeling. The electron suffer acceleration by an electric field, which under the condition $\omega >> \nu_u$ (ν_u energy relaxation frequency) can be written

$$E_{\text{eff}} = \frac{E_0/\sqrt{2}}{\sqrt{(\omega/\nu_m)^2 + 1}} \tag{21}$$

with E_0 field amplitude and ν_m frequency for momentum exchange. In pure N_2 at p = 100 kPa equat. (21) is valid for a microwave frequency $\nu >> 1.3 \cdot 10^9$ 1/s. The population of the vibrational states of N_2, NO or O_2 turns out to be a sensitive function of E(t) and the electron density n_e. The relation between n_e and E on one side and T_{vib} as characteristic parameter of the population densities on the other follows from a model, whose flow sheet is displayed in fig. 9.

CARS experiments on N_2 deliver the important parameter T_{vib}. A comparison between measured and calculated vibrational temperature is shown in fig. 10a for pure N_2. The calculated electron and ion densities are plotted in fig. 10b. Notice that the electron density is nearly completely neutralized by N_4^+ ions, the other charged species are of minor importance.

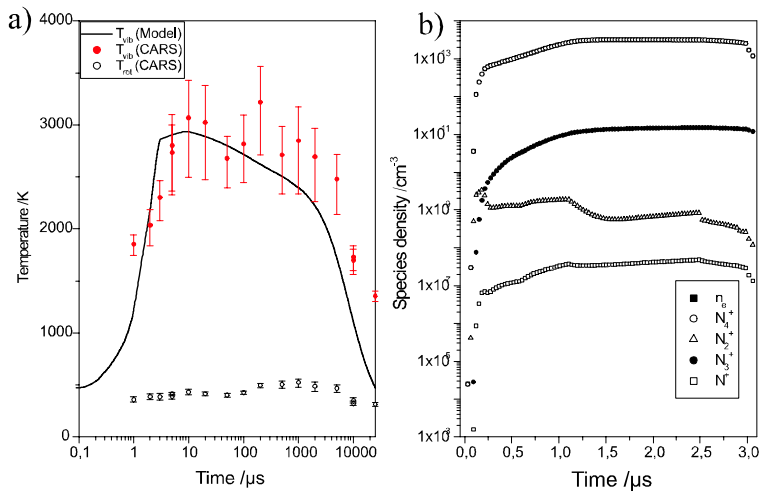

Figure 10.a) Measured and calculated vibrational and gas temperature b) Density of charged particles in pure nitrogen at atmospheric pressure.

4.3 Results from POLCARS experiments

The detection of a minority, e.g. NO in N_2, under atmospheric pressure by CARS is limited to a concentration of 2500 ppm. By applying POLCARS the detection limit can be scaled down to 200 ppm. This technique is used to examine the NO reduction in a reactor chamber fed by vibrationally excited N_2 and by N, which is generated in a cw 2.46 GHz microwave discharge. The N_2 plasma enters the reaction chamber via a nozzle. Behind the nozzle NO is added and decomposed. A setup of this experiment is shown in fig. 11 after [6].

In fig. 12a CARS measurements on 2500 ppm NO in atmospheric N_2 are plotted showing the limit of this detection technique. Contrary to these measurements, POLCARS signals can still be evaluated, see fig. 12b, even down to a concentration of 250 ppm.

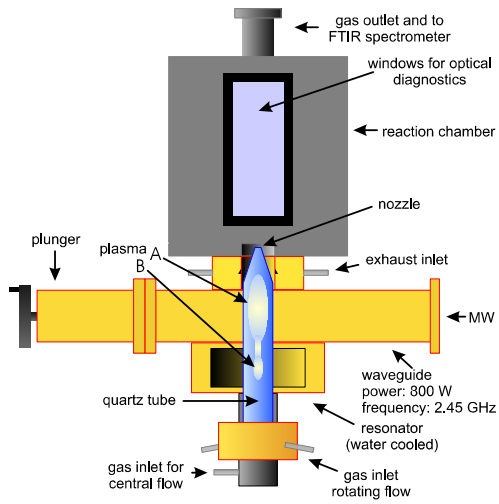

Figure 11. Microwave discharge and reaction chamber

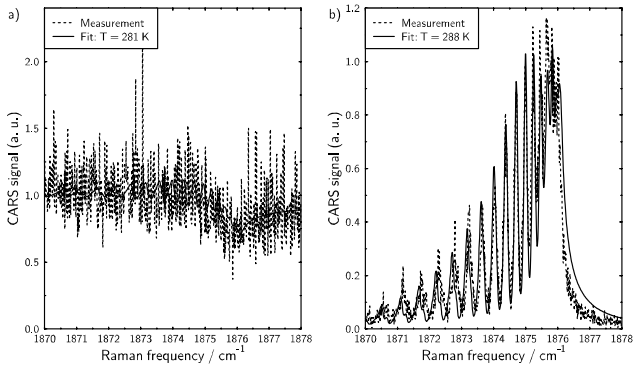

Figure 12. a) CARS spectrum of 2500 ppm NO in N_2 at p = 100 kPa b) POLCARS spectrum under the same conditions as in fig. 12a.

4.4 Results from RECARS measurements

In preparation of RECARS experiments the molecular energy levels and dipole transition moments of the molecule under consideration should be known. In case of InI quantum mechanical calculations has to be performed up to high rotational quantum numbers (J = 200) to meet the requirements of our experiment [7]. In a second step the RECARS spectrum as function of temperature and pressure applying equat. (15) and (16) must be evaluated. Fig. 13a shows a calculated RECARS spectrum of InI under a low pressure (120Pa) compared with the experimental one, see fig. 13b. At high pressure (112 hPa) under presence of mercury the RECARS lines are broadened and overlap, see fig. 14. Here a broadening constant of Γ = 0.23 cm^{-1} is adequate. A local temperature measurement is possible by comparing the ratio of two distinct peaks.

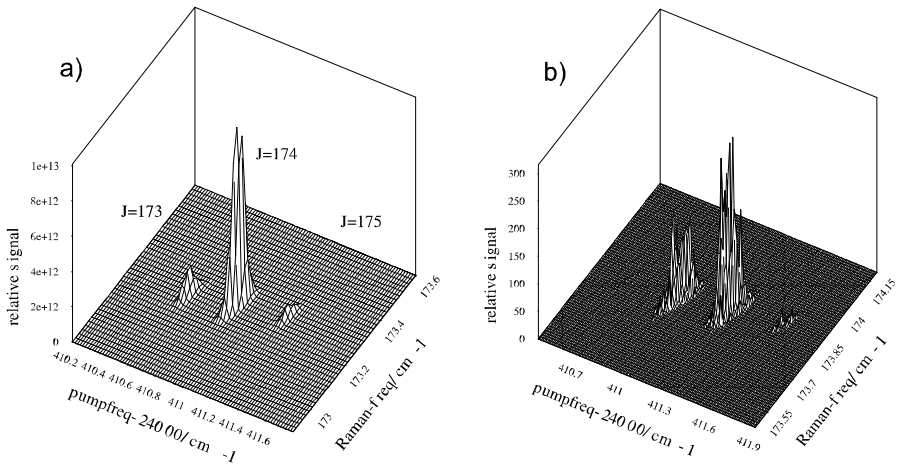

Figure 13. a) Calculated RECARS spectrum of InI (T = 880 K, pressure broadening constant Γ = 0.0025 cm^{-1}) b) Measured RECARS spectrum of InI for the same conditions as in fig. 13a

5 Conclusive remarks

The examples chosen here to explain the CARS technique and its variants substantiate the broad applicability of this diagnostic technique in plasma physics. In particular in low temperature plasmas with a multitude of molecular species this diagnostic technique is unrenounceable. The equilibrium state of the plasma as well as the distribution of produced species can be investigated, even the electron density can be found.

Future experiments on CARS will operate improved laser systems, in particular with respect to beam-pointing stability, spectral width and the wave length regime. A thorough study of CARS line widths

give a lot of information about saturation and collisional broadening. Of interest are experiments with very short laser pulses, which are not discussed here. Also, degenerate four wave mixing is a promising, and still applied technique to diagnose a plasma. This spectroscopic technique becoming more and more popular is distinguished by a greatly enhanced sensitivity plus efficient background suppression. However, the theoretical description has to include saturation, which makes the evaluation cumbersome.

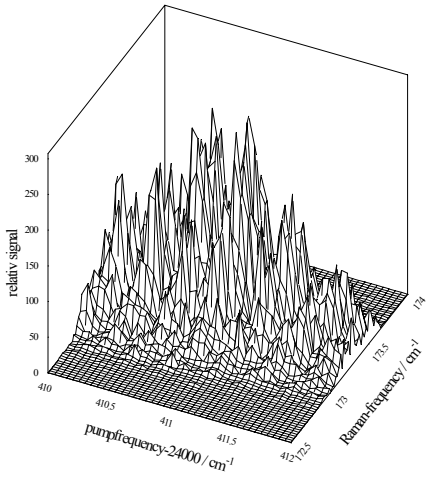

Figure 14. Measured RECARS spectrum of InI in a Hg majority (T = 1073 K, P_{InI} = 1.12 hPa, P_{Hg} = 112 hPa)

References

[1] S.A.J. Druet, J-P. E. Taran, Prog. Quant. Electr. **71-72** (1981) 1

[2] A.C. Eckbreth and R.J. Hall, Combustion Science and Technology, **25** (1981) 175

[3] J.W. Nibler, G. V. Knighten, "Coherent Anti-Stokes Raman Spetroscopy", in "Raman Spectroscopy of Gases and Liquids", Ed.: A. Weber, Springer Verlag Berlin (1979) 253

[4] T. Doerk, J. Ehlbeck, P. Jauernik, H. Kempkens, J. Uhlenbusch in "Lasers - Physics and Appplications", Proc. VI Intern. School on Quantum Electronics, Varna, Bulgaria, Sept. 1990, ed. by P. Atanasov, World Scientific, Singapore (1991) 92

[5] T. Doerk, J. Ehlbeck, R. Jedamzik, J. Uhlenbusch, J. Hoeschele, J. Steinwandel, Appl. Spectr. **51** (1997) 1360

[6] A. Pott, T. Doerk, J. Uhlenbusch, J. Ehlbeck, J. Hoeschele, J. Steinwandel, J. Phys. D: Appl. Phys **31** (1998) 2485

[7] M. Bruchhausen, J. Voigt, T. Doerk, S. Hädrich and J. Uhlenbusch, Journ. of Mol. Spectr. **201** (2000) 70

[8] W.R. Cannon, S.C. Danforth, J.H. Flint, J.S. Haggerty, R.A. Marra, J. Am. Cera. Soc. **65** (1982) 324

[9] M. von Hoesslin, J. Förster, J. H. Schäfer, J. Uhlenbusch: Appl. Phys. **B61** (1995) 367

[10] J. Y. Zhu, D. Dunn-Rankin: Appl. Phys. **B65** (1993) 47

[11] J. Foerster, M. von Hoesslin, J. Uhlenbusch: Appl. Phys. **B62** (1996) 609

[12] B. M. Penetrante, S. E. Schultheis eds.: "Non-thermal plasma technique for pollution control", several contributions concerning gas purification, Springer Berlin (1993)

[13] M. Klein, D. W. Branston, G. Lins, M. Römheld, R. Seeböck, Proc. Int. Conf. on Gas Discharges and their Applications, Tokyo (Sept. 1995), vol **2**, 414.